MDPI

Article

Ab initio generation of binary alloy foams: the case of amorphous $Cu_{64}Zr_{36}$

Jonathan Galván-Colín [1], Ariel A. Valladares [1,*], Alexander Valladares[2], Renela M. Valladares [2]

[1] Instituto de Investigaciones en Materiales, Universidad Nacional Autónoma de México, Apartado Postal 70-360, México, D. F. 04510, México; E-Mails: jgcolin@ciencias.unam.mx (J.G.C.); valladar@unam.mx (A.A.V.)

[2] Facultad de Ciencias, Universidad Nacional Autónoma de México, Apartado Postal 70-542, México, D. F. 04510, México; E-Mail: valladar@ciencias.unam.mx (A.V.); renelavalladares@gmail.com (R.M.V.)

* Author to whom correspondence should be addressed; E-Mail: valladar@unam.mx (A.A.V.); Tel.: +52-55-5622-4636; Fax: +52-55-5622-4636.

Received: 16 April 2016; Accepted: 26 April 2016; Published: 2 May 2016

Abstract: We report *ab initio*-based processes to generate an amorphous nanoporous $Cu_{64}Zr_{36}$ metallic glass. Starting with two different initial configurations: an unstable crystalline sample ($cCu_{64}Zr_{36}$) and an amorphous sample ($aCu_{64}Zr_{36}$), the transferable expanding lattice method– previously used with semiconducting and pure metal systems– was applied in order to increase the volume of the cells (and atomic distances proportionally) so that the density was halved, thus obtaining 50% porosity. The initial samples were subjected to either constant room temperature *ab initio* molecular dynamics or geometry optimization only, which resulted in well-defined pores growing along specific spatial directions. Herewith we report partial and total pair distribution functions, as well as nearest neighbor distances and coordination numbers which let us discern differences in backbone and pore topology. Also we report the bond-angle distribution which let us track the presence of icosahedral-like short-range order which is often related to the glass forming ability in amorphous alloys. The so-called depletion of the pair distribution function at mid range order reported in the literature, along with an estimation of pore sizes are also reported.

Keywords: BMG foam; ab initio; amorphous Cu-Zr; expanding lattice

1. Introduction

Although porous materials have long been used for several purposes, their study remains a cutting-edge topic among material scientists and engineers. Research on these materials does not only involve the ongoing development of techniques to obtain them experimentally–which often becomes onerous when pore size control in the *nano* regime is required–but also to characterize them in order to foster their potential properties [1]. Attention has been focused on amorphous porous metals due to the promising combination of exceptional physical and mechanical properties, for it is desired that microscopic ductility in the structure should improve macroscopic ductility in the amorphous metallic foam [2]. Such amorphous-alloy foams would have other potential applications due to their porous nature; they might be used as fluid nanofilters, high-corrosion and wear resistant structures, adsorption materials, etc. [3].

More than a decade ago, the first successful method to create a bulk metallic glass foam (BMGF) was reported by Schroers *et al*. [4], who prepared a low-density Pd-based alloy $Pd_{43}Cu_{27}Ni_{10}P_{20}$ with closed pores of 200-1000 μm with the aid of hydrated B_2O_3 gas as bubble generator. In 2004, Brothers

and Dunand reported the foaming of a Zr-based alloy by rapid quenching $Zr_{57}Nb_5Cu_{15.4}Ni_{12.6}Al_{10}$, achieving small pore sizes of 25-50 μm [2]. Successive experimental work was mainly focused on multicomponent alloys such as $Ni_{59}Zr_{20}Ti_{16}Si_2Sn_3$ [5], $Fe_{48}Cr_{15}Mo_{14}Y_2C_{15}B_6$ [6] and $Mg_{60}Cu_{21}Ag_7Gd_{12}$ [7], among others.

From the theoretical point of view, not much literature has been published on the modeling approaches for the generation of amorphous porous materials in general, nor for amorphous porous metals in particular. On the whole, either the "reconstructive" or the "mimetic" approaches have been taken. While the former involves the use of constraints obtained from experimental data, the latter implies the simulation of realistic processes to obtain structures which involve a non trivial design [8]. Furthermore there are also the Monte Carlo (MC) and classical molecular dynamics (MD) schemes; in spite of their advantage to handle several thousands of atoms in a simulation cell, they are either focused on reproducing particular experimental data or their applicability is restrained to a single system, as in the mimetic approach. As far as we know, no previous *ab initio* approach has been reported in the literature [8].

One geometric approach that has been used to generate amorphous porous samples is the one where the pore is "manually" carved directly in the simulation cell. However, this biasing in the initial structure influences the resulting porous structure; besides the initial crystalline structure will become distorted only in the vicinity of the porous rather than on the whole. Another method that has been reported recently by Santiago-Cortés *et al.* [9, 10], mimics, to some extent, the dealloying process followed by experimentalists to generate meso and macroporous structures. Also there is another approach that has been used to generate nanoporous semiconducting structures and some pure metallic systems: the expanding lattice (EL) approach reported by Valladares *et al*. [11,12]. Since this method is *ab initio*-based, it excludes the possibility of adding and fitting parameters from experiment and, in principle, leads to *non-manipulated* structures contrary to other approaches, making the method transferable. Withal, it is well-known that *ab initio* methods are computationally onerous and that the number of atoms that can be handled is no greater than a few hundred. Therefore in order to properly describe any property of the material, a study with a large number of atoms is often desired so that it can be representative. The EL method has proven to reproduce some properties in amorphous nanoporous carbon [13]. Since the method has been used only with pure elements so far, it is desirable to investigate its application to alloys especially to amorphous ones with simple compositions such as those of the binary type.

Herewith, we report the use of the EL approach to generate amorphous nanoporous $Cu_{64}Zr_{36}$ with 50% porosity. We chose this alloy because it has a simple atomic composition, and its topology in the amorphous phase has been widely studied in the literature [14-19]. We present a structural analysis by means of the pair distribution function (PDF) so that the local atomic environment can be characterized along with the bond-angle distribution (BAD) which let us track the percentage of icosahedral-like short-rage order (SRO), which is often related to the glass forming ability of the bulk and its mechanical properties. In addition, we compare the resulting porous samples with previously reported non-porous structures to trace relevant structural changes due to porosity.

2. Method

In order to generate amorphous nanoporous $Cu_{64}Zr_{36}$ alloys we take two paths, one which involves a thermal stage with *ab initio* molecular dynamics (AIMD) plus geometry optimization, and another one just involving a geometry optimization (GEOPT).

First, we start from two initial cubic supercells with 108 atoms, i.e., 69 Cu atoms and 39 Zr atoms: an amorphous cubic supercell (a-$Cu_{64}Zr_{36}$), whose generation details are fully commented elsewhere [20-22]; and second, from an unstable crystalline configuration (c-$Cu_{64}Zr_{36}$) selected in order to foster disorder during the molecular dynamics process. The EL method is applied then to each sample using the following relation: $l_2 = 2^{1/3} l_1$, where l_2 is the edge of the expanded cell and l_1 is the initial edge of

the supercell [11]; this lowers the density from 8.06 g/cm^3 to 4.03 g/cm^3 (Fig. 1) in order to reach 50% porosity.

This percentage was chosen in order to avoid either short lattice expansions that might lead to high crystalline remnants in c-$Cu_{64}Zr_{36}$, or weak interactions among atoms in the supercell due to large lattice expansions [9].

2.1. AIMD

Once we had the expanded samples, they are subjected to constant temperature AIMD at 300 K (room temperature). The NVT ensemble with a Nose-Hoover thermostat is used as well as the Verlet velocity integrator algorithm. The MD process is carried out for 500 simulation steps using a time step of 10.71 fs. After the constant temperature stage, the samples are relaxed by means of a geometry optimization in order to reach their corresponding energy minimum.

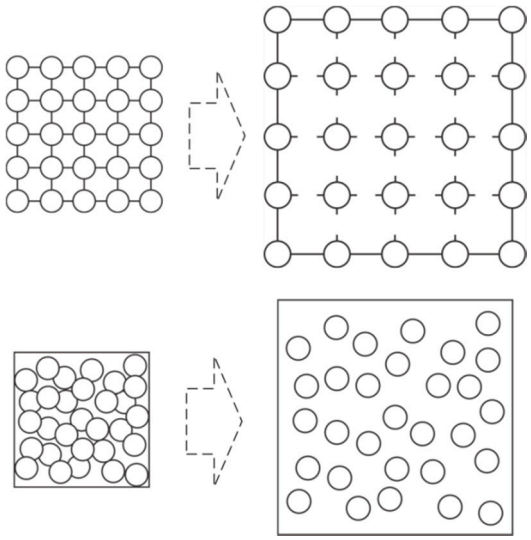

Figure 1. Schematic representation of the initial supercells subjected to the lattice expansion method (EL).

2.2. GEOPT

The second alternative to generate the amorphous nanoporous structure is based on the initially expanded structures (a-$Cu_{64}Zr_{36}$ and c-$Cu_{64}Zr_{36}$) and then relaxing them via geometry optimization only, thus excluding the temperature factor. This would lead the system to reach its minimum energetic configuration. This approach was chosen since it is well-known that in alloys atomic radii differences reduce atomic mobility (hence preventing the formation of crystalline phases) thereby leading to the formation of the amorphous.

All simulations are performed using DMol^3, a density-functional-based code which builds the atomic orbitals via a linear combination [23, 24]. Furthermore, within the local density approximation the Perdew-Wang exchange and correlation functional is used [25]. The calculations are performed unrestricted using double-numerical atomic basis sets with d polarization functions (dnd) along with cut-off radii of 4.4 Å for Cu and 5.3 Å for Zr. Since *ab initio* methods are known to be computationally demanding, to optimize the CPU time we use the DFT semicore pseudopotentials (dspp) [26], which replaces the core electrons with a simple potential and adds a certain degree of relativistic effects on them.

To characterize the local atomic environment, we calculate the partial coordination numbers N_i by integrating the partial PDFs up to the first corresponding minimum r_c. Once we have the partial coordination numbers, we add them in order to get the total coordination numbers of every

amorphous porous sample. Furthermore, by using the first minima r_c as the interatomic distances we calculate the BAD to track either the possible remnants, or the presence of icosahedral-like SRO.

We must make clear that in our approach we do not pretend to mimic the experimental processes by which amorphous nanoporous alloys are grown, but we want to devise a theoretical approach which allows us to generate reliable structures that could represent the experimental ones. It is worth mentioning that since experimental PDF information has not been reported yet for amorphous porous Cu-Zr the results presented here should be considered predictive.

3. Results and Discussion

Figures 2-5 present the resulting amorphous nanoporous structures as viewed from several axial directions, where we can notice that through-pores grew along well defined spatial directions. We see that there is no obvious relation among the different growing directions in all four samples. However we can say that at least in every sample there is a spatial direction along which dendritic-like topology is clearly observed, e.g., both Fig. 2b and 3b show a tree-like backbone, although the orientation differs, while Fig. 4c and 5c have dendritic-like topology. Moreover, we see that there are certain similarities for those structures that started from a-$Cu_{64}Zr_{36}$, up to some extent, which is not the case for the ones that started from c-$Cu_{64}Zr_{36}$. Thus, we can notice that pore size and topology strongly depends on the initial structure and the porous process. We also observed that minor pores appear different spatial directions.

We denote the structures generated by GEOPT as: ap-c-OPT and ap-a-OPT; while the ones generated by AIMD as: ap-c-AIMD and ap-a-AIMD. In Figures 6a-c we show the three partial pair distribution functions (pPDFs) of our four resulting samples.

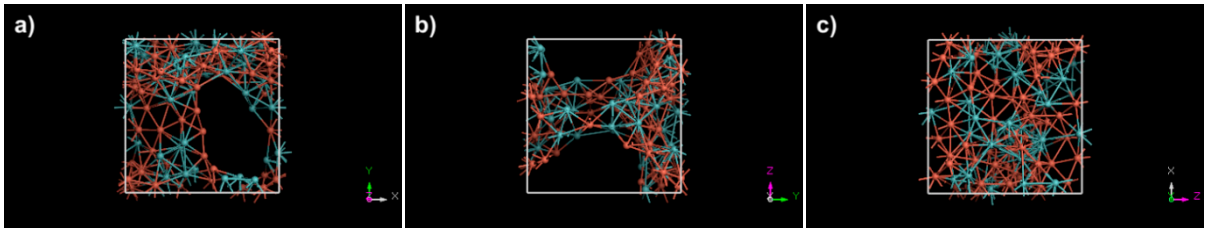

Figure 2. Ball-and-stick resulting amorphous nanoporous sample with initial c-$Cu_{64}Zr_{36}$ structure generated by GEOPT (ap-c-OPT). (**a**) xy plane view. (**b**) yz plane view. (**c**) zx plane view. Cu atoms are depicted in red and Zr atoms are in blue. Bonds are represented as rods.

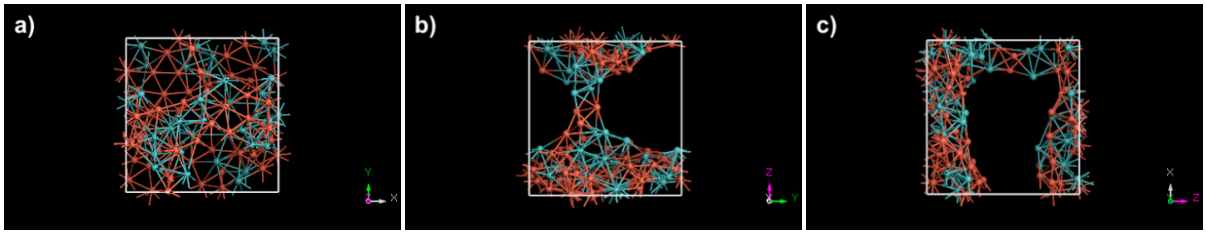

Figure 3. Ball-and-stick resulting amorphous nanoporous sample with initial a-$Cu_{64}Zr_{36}$ structure generated by GEOPT (ap-a-OPT). (**a**) xy plane view. (**b**) yz plane view. (**c**) zx plane view. Cu atoms are depicted in red and Zr atoms are in blue. Bonds are represented as rods.

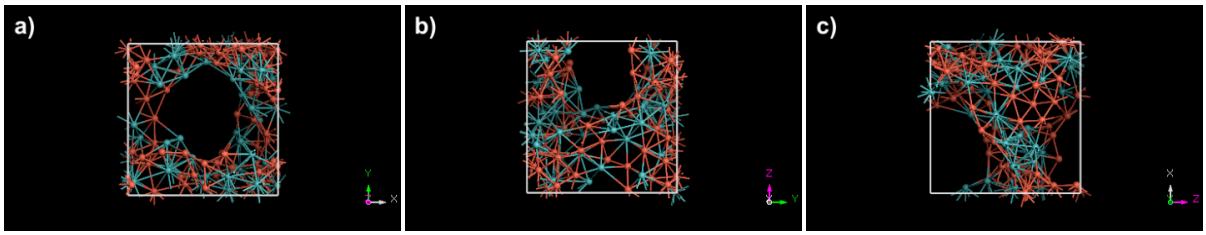

Figure 4. Ball-and-stick resulting amorphous nanoporous sample with initial c-$Cu_{64}Zr_{36}$ structure generated by AIMD (ap-c-AIMD). (**a**) xy plane view. (**b**) yz plane view. (**c**) zx plane view. Cu atoms are depicted in red and Zr atoms are in blue. Bonds are represented as rods.

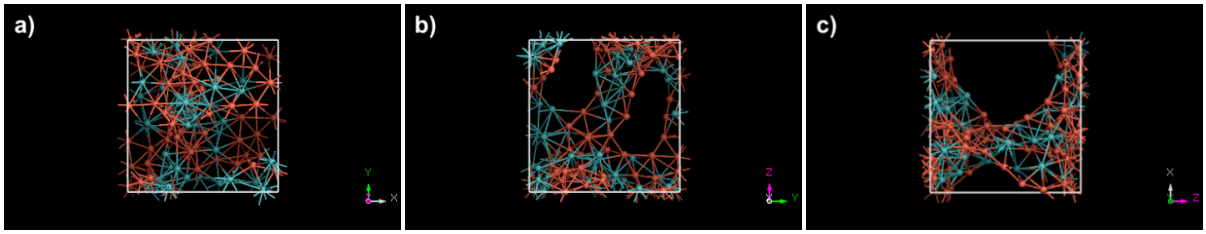

Figure 5. Ball-and-stick resulting amorphous nanoporous sample with initial a-$Cu_{64}Zr_{36}$ structure generated by AIMD (ap-a-AIMD). (**a**) xy plane view. (**b**) yz plane view. (**c**) zx plane view. Cu atoms are depicted in red and Zr atoms are in blue. Bonds are represented as rods.

It can be noticed that in Cu-Cu and Cu-Zr pPDFs there is a good agreement among all samples up to a distance of about 6 Å, which is not the case of Zr-Zr partial since Zr is the less abundant atomic species in the system and fluctuations arise. Despite these short-range order variations, in all three pPDFs the bimodal second peak which is often related to metallic glasses can be observed [27]. In addition, the samples which were initially crystalline, regardless of the process, become fully amorphous according to their corresponding PDFs. As previously recognized by Santiago-Cortés *et al*. [10, 11], we show as insets in Figures 6a-c the depletion of the PDF which will be discussed later and which is a consequence of the porosity in the samples.

The agreement of the PDFs in all our generated amorphous porous alloys can also be confirmed via the first neighbor positions (r_1) from Table 1. We can see that they all agree within 2% and compared with the non-porous amorphous $Cu_{64}Zr_{36}$ (denoted as *np*-a-$Cu_{64}Zr_{36}$) they are somewhat smaller. We believe that in porous amorphous metals, the displacement to shorter distances of the first neighbor positions in the porous PDFs could be related to atoms located near the pore surface; since they are not in the bulk there is an asymmetry in the interactions exerted by the surrounding atoms that attract surface atoms closer to them (to compensate for the lack of atoms in the pore), thereby diminishing their interatomic distance 8% at most.

As for the total PDFs (Figs. 7a-b), the GEOPT-generated structures are practically the same while AIMD-generated differ in height, not in, shape up to the second coordination shells. Nevertheless, it is worth mentioning that from the third coordination shell ap-c-AIMD and ap-a-AIMD structures differ due to a left displacement of the latter, which means that the structure whose initial configuration is the unstable crystal has peaks located at positions that resemble more the non-porous amorphous $Cu_{64}Zr_{36}$ peak positions; in other words, the final ap-c-AIMD structure–although having the same porosity percentage–has smaller pores than the other samples which can be seen in its resulting topology depicted in Figures 4a-c. When comparing the total PDFs with the non-porous amorphous $Cu_{64}Zr_{36}$ we see that there is an evident difference in height due to the change in the number density ρ_0 upon volume increase. We believe that these differences between ap-c-OPT and ap-a-OPT, and ap-c-AIMD and ap-a-AIMD are associated with the initial configuration, i.e., it might be energetically

favorable to start with an amorphous structure rather than an unstable crystalline which would have to be disordered in the first place and become porous afterwards. However, these variations are not relevant when considering SRO via the coordination numbers (N_i) in Table 1.

Table 1. Partial and total first-neighbor positions (r_i) and coordination numbers (N_i) of amorphous nanoporous $Cu_{64}Zr_{36}$ obtained by GEOPT and AIMD processes.

	r_{Cu-Cu}	r_{Cu-Zr}	r_{Zr-Zr}	r_{Total}	N_{Cu-Cu}	N_{Cu-Zr}	N_{Zr-Cu}	N_{Zr-Zr}	N_{Cu}	N_{Zr}	N_{Total}
ap-c-OPT	2.43	2.68	2.98	2.58	4.5	3.8	6.7	3.7	8.3	10.4	9.0
ap-a-OPT	2.43	2.73	2.93	2.58	4.8	3.7	6.6	3.7	8.5	10.3	9.1
ap-c-AIMD	2.43	2.73	2.98	2.58	4.4	3.8	6.7	4.2	8.2	10.9	9.1
ap-a-AIMD	2.48	2.68	2.93	2.58	4.6	3.5	6.2	4.1	8.1	10.3	8.9
np-a-$Cu_{64}Zr_{36}$	2.45	2.75	3.15	2.70	6.7	5.3	9.4	6.3	12	15.7	13.2

In the case of the first coordination shell locations, first neighbor distances –although varying somewhat– have an acceptable agreement for all four amorphous nanoporous structures; the highest variation is of 10% in the case of N_{Zr-Zr}, which is again related to the fluctuations caused by the small number of atoms in the supercells. Thus, it would be desirable to have a larger atomic system in order to diminish fluctuations and have better descriptions of the system, statistically speaking; nonetheless, our group has formerly proven that the PDF of a 64-atom amorphous silicon system compared with the corresponding one of 216-atom are practically the same [28].

An important feature related to coordination numbers is that they all exhibit a clear drop of about 2 for partial N_is and of 4 for total Ns. We consider that a consequence of this lowering is also related to the presence of pores in the simulation cell. On one hand we have the atoms located in the backbone or the "bulk", and on the other hand the atoms located at the surface of the pore. Since surface increases as porosity does, there is a competence between the backbone atoms that contribute to coordination and the voids inherent to the pores formed.

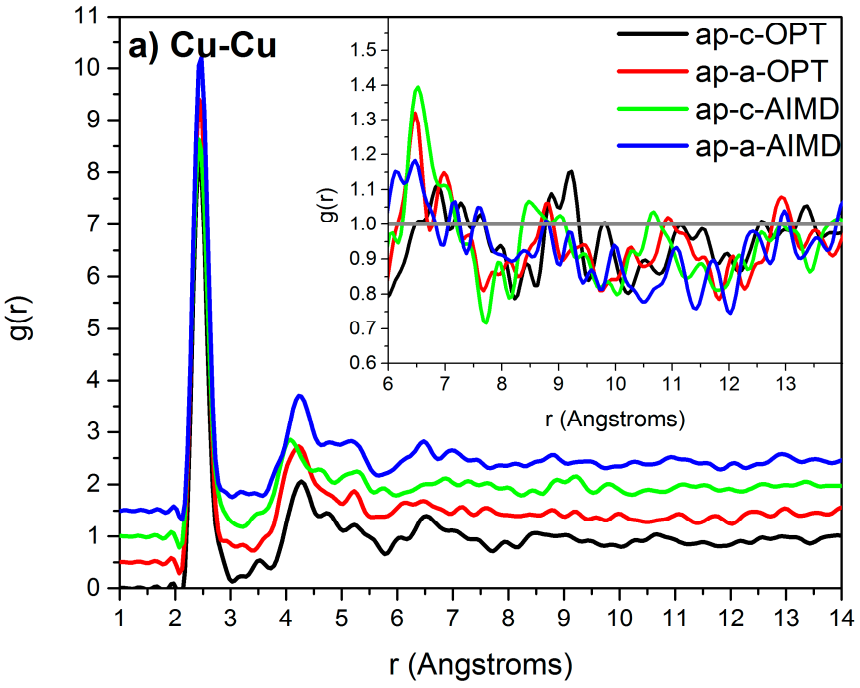

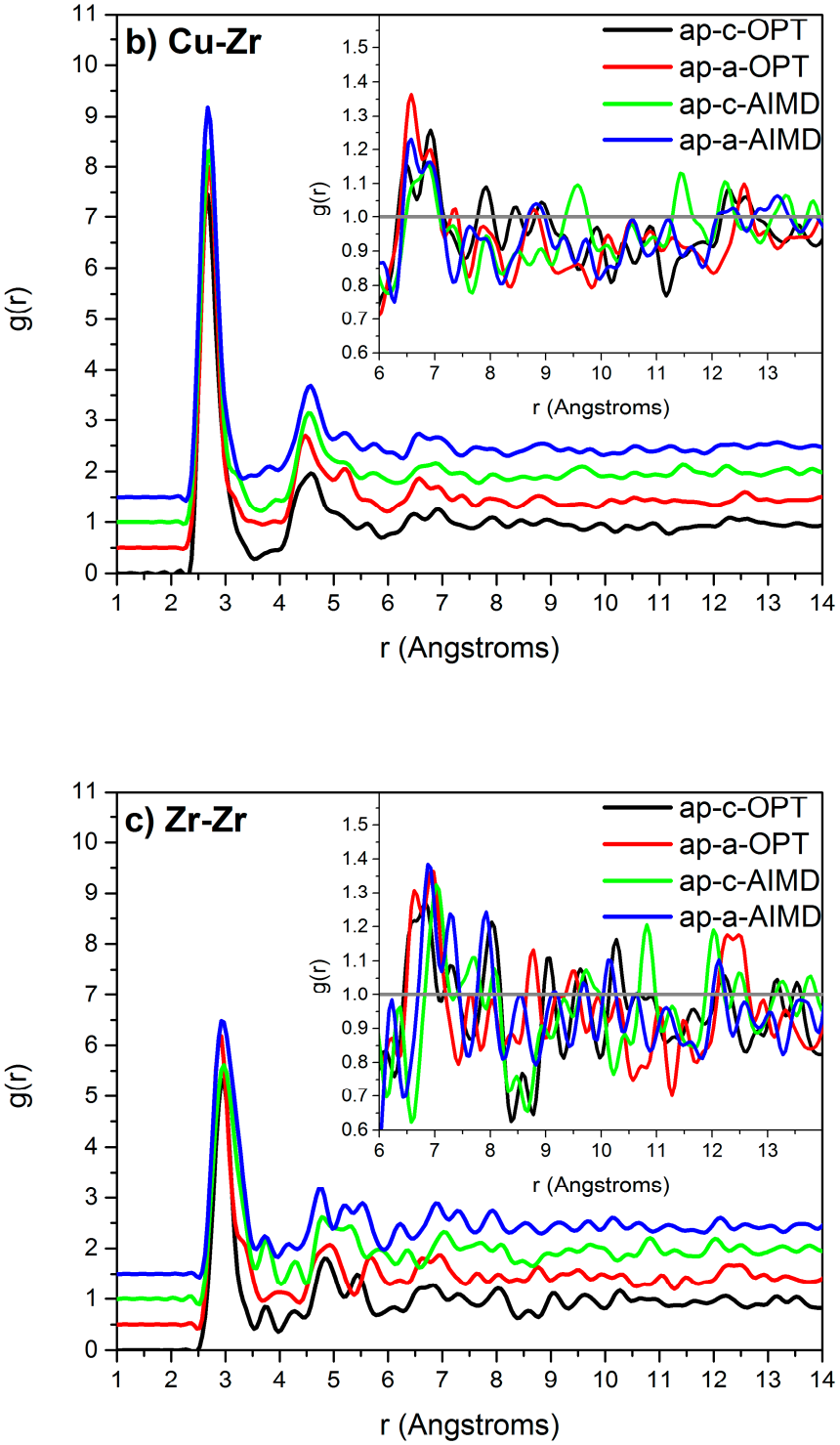

Figure 6. Partial pair distribution functions of amorphous nanoporous $Cu_{64}Zr_{36}$ generated by GEOPT and AIMD: (**a**) Cu-Cu. (**b**) Cu-Zr. (**c**) Zr-Zr. The insets show the depletion of the PDF as a consequence of porosity in the resulting structure. For a better comparison among the curves, they were shifted along the *y* direction.

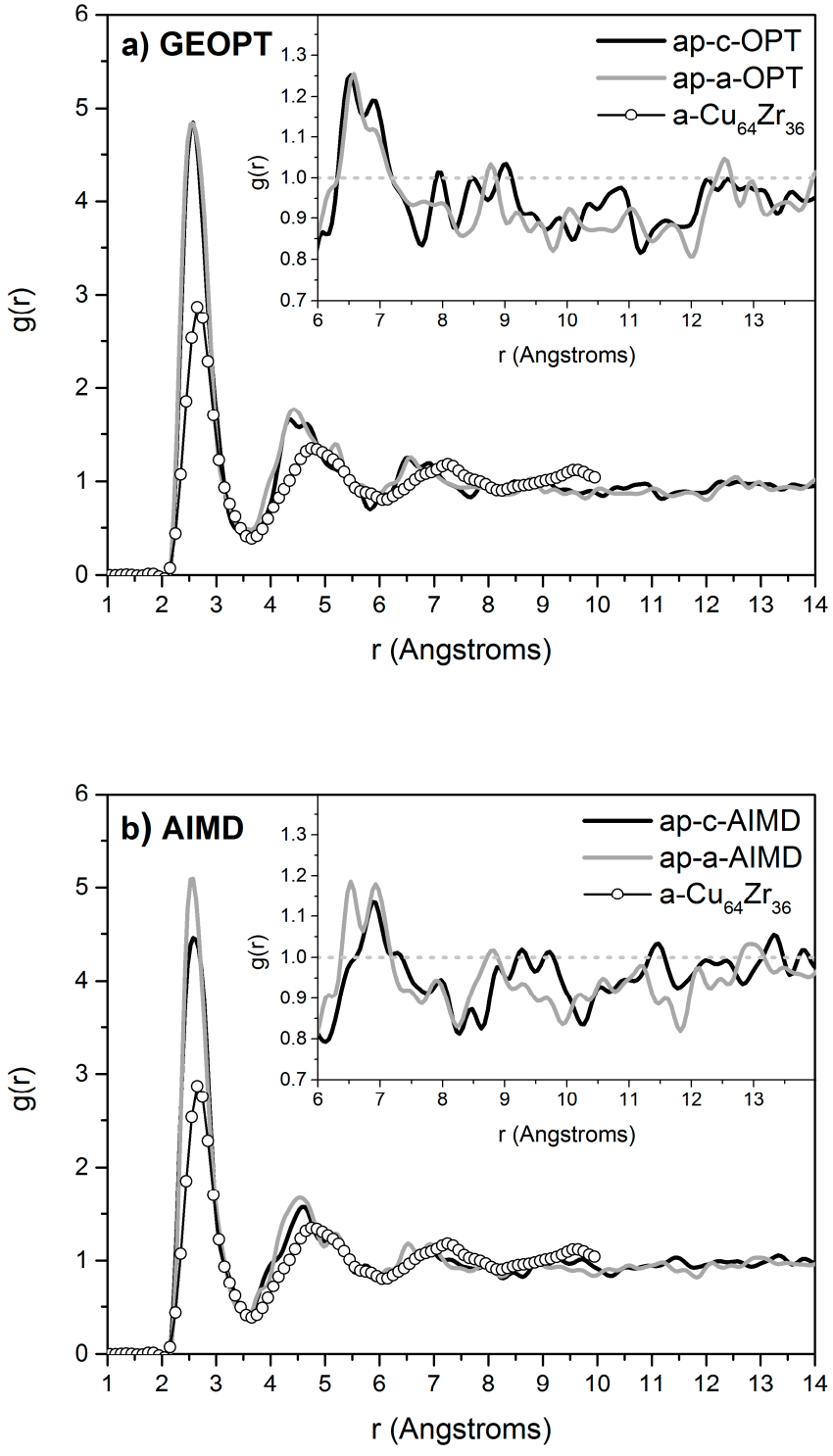

Figure 7. Total pair distribution functions of amorphous porous $Cu_{64}Zr_{36}$ generated by (**a**) GEOPT; and (**b**) AIMD. The hollow circles represent non-porous amorphous $Cu_{64}Zr_{36}$ from Ref. [16]. The corresponding insets show the depletion of the PDF as a consequence of porosity in the resulting structure.

As was previously mentioned, the depletion in the PDF has its origin in the pores within the supercell in pure amorphous nanoporous materials [9]. Moreover, it depends on the topology of the pores since a homogeneous distribution of them in the simulation cell would lead to a dendritic-like structure and no noticeable depletion of the PDF. In the case where the backbone and the pore are localized, i.e., the pore is concentrated in a region of the simulation cell, the depletion shows up and it prevails as porosity increases. Furthermore, at this stage we can estimate the size of the pore by determining the distance range in which the depletion of the total PDFs spreads; nevertheless, setting the depletion limits is not a trivial task due to fluctuations in the PDF. For this reason, we decided to perform a Fast Fourier Transform smoothing in order to discard high frequencies and devise a way that could let us estimate the limits of the depletion (Figs. 8a-b).

From Figures 8a-b, we estimate the pore size by measuring the distance range where the PDFs remained systematically below 1 beyond the third neighbor coordination peak. These results are shown in Table 2.

Since the coordination numbers from Table 1 do not provide enough evidence of the presence of icosahedral-like SRO, we computed the total BAD of our four amorphous porous samples which are shown in Figures 9a-b. Comparisons with the non-porous amorphous $Cu_{64}Zr_{36}$ and the angles of an ideal icosahedron are shown as well.

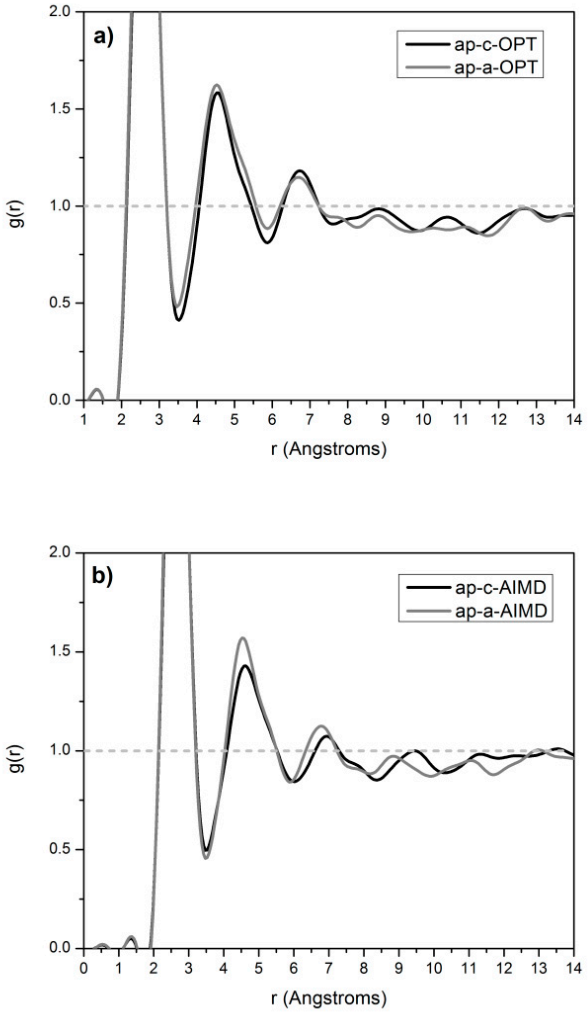

Figure 8. Fast-Fourier-Transform smoothing of the total PDFs performed to show the spread of the depletion and to relate it with the pore size. (**a**) GEOPT. (**b**) AIMD.

Table 2. Pore size estimation from the depletion observed in the total PDFs in Figs. 8a-b. In ap-c-AIMD simulation there is a peak at 9.43 Å whose *g(r)* value is 0.9994 considered as 1, thus we measured two pore sizes.

Simulation	Pore size [Å]
ap-c-OPT	7.1
ap-a-OPT	7.5
ap-c-AIMD	2.1, 3.9
ap-a-AIMD	5.6

We can see from Fig. 9a-b that despite having well-defined peaks that might be related to icosahedral-like SRO, the number of angles present in the porous samples compared to the ones in the non-porous amorphous are systematically smaller over the whole range of the BAD. We think that this behavior is also a consequence of the backbone and pore competition; i.e., the number of bulk atoms is reduced upon pore formation. Moreover, GEOPT-generated porous samples tend to form more distorted geometries since the second bump of the BAD is more spread, whereas the AIMD-generated samples exhibit a more localized second bump around the value of 108° which is related to the inner angles of a pentagon. We also see that the first peak around 60° in the case of the AIMD-generated samples shows contributions due to angles whose values can be either smaller or larger than 60°.

Although we cannot assert whether icosahedral-like SRO dominates in our amorphous porous samples, we can say that AIMD-generated structures have geometries which resemble more an icosahedral-like one, qualitatively. Furthermore, we can also mention that since the prevailing peak in all BADs is located around 60°, the geometries present in our porous samples should be triangle-like. Thus, we think that such geometries are associated to the Frank and Kasper (FK) polyhedra *Zn*: the so called *triangulated coordination shells* [29]; of course, the geometries in our samples are not ideal but rather distorted or truncated since we have smaller coordination numbers compared to the non-porous amorphous structure, manifesting again pore growing, backbone formation and an increasing surface.

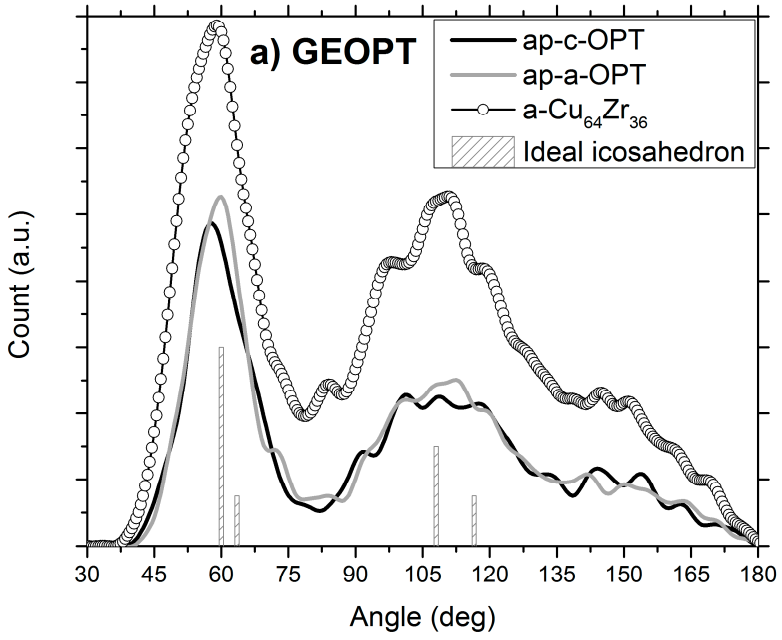

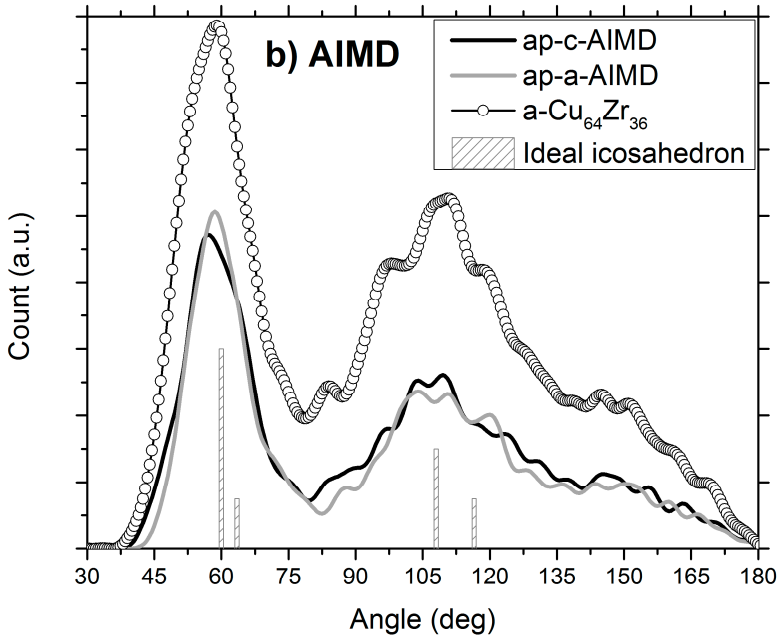

Figure 9. Bond-angle distribution of amorphous porous $Cu_{64}Zr_{36}$ generated by (**a**) GEOPT; and (**b**) AIMD. The hollow circles represent non-porous a-$Cu_{64}Zr_{36}$ from Ref. [16].

We see that there are two tendencies in pore size among our results: a) pores in AIMD-generated structures are smaller than those present in GEOPT-generated samples; and b) pores in structures that started from c-$Cu_{64}Zr_{36}$ are smaller than those whose initial structure was a-$Cu_{64}Zr_{36}$. This implies the following key points about the generation of amorphous nanoporous structures with these approaches: a) amorphous nanoporous alloys generated from an unstable crystalline cell have a larger backbone size, thus a smaller pore due to a possible high energetic cost of disordering the structure after the lattice expansion with the AIMD generation process; b) smaller coordination numbers (compared to the non-porous amorphous $Cu_{64}Zr_{36}$) are not significant to assert whether our samples have or do not have icosahedral-like SRO, for we have mentioned above that such lowering in N_i is related to a competition between pores and bulk contributions; however, from the BADs we can assert the presence of either distorted or truncated FK polyhedra; further analysis of the topology is needed to clarify this point; c) since there is not an apparent relation between the generation processes and the resulting pore topologies, a larger simulation cell would help to discern whether pore topology is cell-size dependent giving a better insight to the formation of these materials.

4. Conclusions

We proposed two *ab initio*-based approaches to generate amorphous nanoporous structures of $Cu_{64}Zr_{36}$ alloy based on the expanding lattice method; one approach involves *ab initio* molecular dynamics; and another one involving geometry optimization only, thus discarding the temperature factor. By using different initial configurations (a-$Cu_{64}Zr_{36}$ and c-$Cu_{64}Zr_{36}$) we noticed that they resemble each other on the whole; however, analyzing the corresponding total PDFs peaks the resulting structures indicate that the unstable crystalline cell does not fully amorphize. This implies slightly thicker backbones and smaller pore sizes, contrary to those samples that started from an amorphized structure. The depletion of the PDF appeared in our analysis, and it was used to get a coarse calculation of the size of the pores in our resulting samples; we think that a larger sample is needed to see whether pore topology is dependent on the cell size and to reduce PDF fluctuations in

order to have a more precise estimation of the depletion range. Certainly, this criterion is a function of the nature of the pore since large *through* pores would contribute more to this depletion than dendritic pores. Further studies at higher temperatures may improve amorphization in AIMD-generated c-$Cu_{64}Zr_{36}$ samples. From the bond-angle distributions we noticed that the porous samples exhibited a similar behavior as the non-porous structure suggesting the presence of icosahedral-like SRO; nevertheless, such geometry does not prevail, for other geometries related to either distorted or truncated FK *Zn* polyhedra might appear. Therefore, better characterization of the local atomic environment in our amorphous nanoporous samples is needed. We look forward to the moment in which binary bulk metallic glass foams are generated experimentally due to their potential applications and to get a better understanding of the mechanisms that originate these promising materials. We think that this work could contribute as incentive to the modeling of amorphous nanoporous alloys from an *ab initio* point of view, which has scarcely been addressed.

Acknowledgments: J.G.C. acknowledges CONACyT for supporting his Ph.D. studies. A.A.V., A.V. and R.M.V. thank DGAPA-UNAM for continued financial support to carry out research projects IN101798, IN100500, IN119105, IN119908, IN112211 and IN110914. M.T. Vázquez and O. Jiménez provided the information requested. Simulations were partially carried out in the Computing Center of DGTIC-UNAM.

Conflicts of Interest: Declare conflicts of interest or state "The authors declare no conflict of interest." Authors must identify and declare any personal circumstances or interest that may be perceived as inappropriately influencing the representation or interpretation of reported research results. Any role of the funding sponsors in the design of the study; in the collection, analyses or interpretation of data; in the writing of the manuscript, or in the decision to publish the results must be declared in this section. If there is no role, please state "The founding sponsors had no role in the design of the study; in the collection, analyses, or interpretation of data; in the writing of the manuscript, and in the decision to publish the results".

References

1. Banhart, J. Manufacture, characterization and application of cellular metals and metal foams. *Prog. Mater. Sci.* **2001**, *46*, 559-632.
2. Brothers, A.H.; Dunand, D.C. Syntactic bulk metallic glass foam. *App. Phys. Lett.* **2004**, *84*, 1108-1110.
3. Brothers, A.H.; Dunand, D.C. Amorphous metal foams. *Scripta Mater.* **2006**, *54*, 513-520.
4. Schroers, J.; Veazey, C.; Johnson, W.L. Amorphous metallic foam. *App. Phys. Lett.* **2003**, *82*, 370-372.
5. Lee, M.H.; Sordelet, D.J. Synthesis of bulk metallic glass foam by powder extrusion with a fugitive second phase. *App. Phys. Lett.* **2006**, *89*, 0219211-3.
6. Demetriou, M.D.; Duan, G.; Veazey, C.; De Blauwe, K.; Johnson, W.L. Amorphous Fe-based metal foam. *Scripta Mater.* **2007**, *57*, 9-12.
7. Brothers, A.H.; Dunand, D.C.; Zheng, Q.; Xu, J. Amorphous Mg-based metal foams with ductile hollow spheres. *J. App. Phys.* **2007**, *102*, 0235081-6.
8. Gelb, L. D. Modeling amorphous porous materials and confined fluids. *MRS Bulletin* **2009**, *34*, 592-601.
9. Santiago-Cortés, C.U.; Mejía-Mendoza, L.M.; Valladares, R.M.; Valladares, A.; Valladares, A.A. Computational alternatives to generate amorphous nanoporous structures using *ab initio* molecular dynamics. *J. Non-Cryst. Solids* **2012**, *358*, 596-603.
10. Santiago-Cortés, C.U. Simulación de sistemas metálicos amorfos y porosos de elementos nobles, Ph.D. Thesis, Universidad Nacional Autónoma de México, México, 2011.
11. Valladares, A.A.; Valladares, A.; Valladares, R.M. Computer modeling of nanoporous materials: An *ab initio* novel approach for silicon and carbon. *Mater. Res. Soc. Symp. Proc.* **2007**, *988*, QQ09-15.
12. Romero, C.; Noyola, J.C.; Santiago, U.; Valladares, R.M.; Valladares, A.; Valladares, A.A. A new approach to the computer modeling of amorphous nanoporous structures of semiconducting and metallic materials: A Review. *Materials* **2010**, *3*, 467-502.
13. Romero, C.; Valladares, A.A.; Valladares, R.M.; Valladares, A. Electronic and vibrational densities of states of *ab initio* generated nanoporous carbons. *J. Non-Cryst. Solids* **2013**, *362*, 14-19.

14. Xu, D.; Lohwongwatana, B.; Duan, G.; Johnson, W.L.; Garland, C. Bulk Metallic glass formation in binary Cu-rich alloys series – $Cu_{100-x}Zr_x$ (x = 36, 36, 38.2, 40 at%) and mechanical properties of bulk $Cu_{64}Zr_{36}$. Acta Mater. **2004**, 52, 2621-2624.
15. Wang, D.; Li, Y.; Sun, B.B.; Sui, M.L.; Lu, K.; Ma, E. Bulk metallic glass formation in the binary Cu-Zr system. Appl. Phys. Lett. **2004**, 84, 4029–4031.
16. Wang, W.H.; Lewandowski, J.J.; Greer, A.L.; J. Understanding the glass-forming ability of Cu50Zr50 alloys in terms of a metastable eutectic. Mater. Res. **2005**, 20, 2307–2313.
17. Duan, G.; Xu, D.; Zhang, Q.; Zhang, G.; Cagin, T.; Johnson, W.L.; Goddard, W.A. Molecular dynamics study of the binary $Cu_{46}Zr_{54}$ metallic glass motivated by experiments: Glass formation and atomic-level structure. Phys. Rev. B **2005**, 71, 2242081–2242089.
18. Mattern, N.; Jóvari, P.; Kaban, I.; Gruner, S.; Elsner, A.; Kokotin, V.; Franz, H.; Beuneu, B.; Eckert, J. Short-range order of Cu-Zr metallic glasses. J. Alloys Compd. **2009**, 485, 163–169.
19. Wang, X.D.; Yin, S.; Cao, P.; Jiang, J.Z.; Franz, H.; Jin, Z.H.; Atomic structure of binary $Cu_{64.5}Zr_{35.5}$ bulk metallic glass. Appl. Phys. Lett. **2008**, 92, 0119021–0119023.
20. Valladares, A.A.; Díaz-Celaya, J.A.; Galván-Colín, J.; Mejía-Mendoza, L.M.; Reyes-Retana, J.A.; Valladares, R.M.; Valladares, A.; Alvarez-Ramirez, F.; Qu, D.; Shen, J. New approaches to the computer simulation of amorphous alloys: A review. *Materials* **2011**, *4*, 716-781.
21. Galván-Colín, J.; Valladares, A.A.; Valladares, A.; Valladares, R.M. Structural and electronic properties of $Cu_{64}Zr_{36}$ BMG by *ab initio* molecular dynamics. *Mater. Res. Soc. Symp. Proc.* **2013**, *1517*, DOI: 10.1557/opl.2012.1757.
22. Galván-Colín, J.; Valladares, A.A.; Valladares, A.; Valladares, R.M. Short-range order in *ab initio* computer generated amorphous and liquid Cu-Zr alloys: a new approach, *Physica B* **2015**, 475, 140-147.
23. $DMol^3$, Materials Studio Suite© v.6.0, Accelrys Inc. 2011.
24. Delley, B. An all-electron numerical method for solving the local density functional for polyatomic molecules. *J. Chem. Phys.* **1990**, *92*, 508-517; Delley, B. From molecules to solids with the $DMol^3$ approach. *J. Chem. Phys.* **2000**, *113*, 7756-7764.
25. Perdew, J.P.; Wang, Y. Accurate and simple analytic representation of the electron-gas correlation energy. *Phys. Rev. B* **1992**, *45*, 13244-13249.
26. Delley, B. Hardness conserving semilocal pseudopotentials. *Phys. Rev. B* **2002**, *66*, 1551251-9.
27. Waseda, Y. *The structure of non-crystalline materials*, McGraw Hill, USA, 1990; pp. 90.
28. Valladares, A.; Valladares, R.M.; Alvarez-Ramírez, F.; Valladares, A.A. Studies of the phonon density of states in ab initio generated amorphous structures of pure silicon. *J. Non-Cryst. Solids* **2006**, *352*, 1032-10136.
29. Frank, F.C.; Kasper, J. S. Complex alloy structures regarded as sphere packings. I. Definitions and basic principles. *Acta. Cryst.* **1958**, *11*, 184-190; Frank, F.C.; Kasper, J. S. Complex alloy structures regarded as sphere packings. II. Analysis and classification of representative structures. *Acta. Cryst.* **1959**, *12*, 483-499.